Bulletin of the Seismological Society of America, Vol. 69, No. 6, pp. 1671–1691, December 1979

TIME-DOMAIN ATTENUATION MEASUREMENTS FOR FUNDAMENTAL SPHEROIDAL MODES ($_0S_6$ TO $_0S_{28}$) FOR THE 1977 INDONESIAN EARTHQUAKE

By Robert J. Geller and Seth Stein

ABSTRACT

Using ultra-long period records of the 1977 Indonesian earthquake from seven IDA stations, we have measured the attenuation of fundamental spheroidal modes from $_0S_6$ to $_0S_{28}$. We determine the attenuation of each mode using a time domain technique which minimizes the effects of noise on the measurements. These measurements are the first attenuation data for these modes from multiple ultra-long period records of a single earthquake. Our results are in good general agreement with single station attenuation measurements from the UCLA gravimeter records of the Alaskan earthquake. They show systematically lower Q^{-1}(less attenuation) than results from stacking WWSSN records.

Introduction

A major goal of current research in long-period seismology is the study of the attenuation of seismic waves in the Earth. The first step in determining the Earth's attenuation structure, as a function of depth and (possibly) frequency and in searching for possible lateral heterogeneity, is making accurate measurements of the attenuation of normal modes, surface waves, and body waves. Different data are best suited for gross Earth attenuation measurements in different frequency bands.

For periods between 20 and about 300 sec, attenuation is best measured from the decay of traveling surface waves (Tsai and Aki, 1969; Kanamori, 1970; Mitchell *et al.*, 1976; Mills and Hales, 1977, 1978a, b; Mills, 1978; Nakanishi, 1978). At periods longer than about 250 or 300 sec, attenuation may be most accurately determined by studying the decay of individual modes.

Periods longer than 300 sec are near or beyond the limits of the response of conventional seismometers like those of the WWSSN. Although it is possible to study some of these periods using the WWSSN records of great earthquakes (e.g., the 1964 Alaskan earthquake), such results are subject to large uncertainties. Other observations in this band have been made using the Isabella strainmeter record of the 1960 Chilean earthquake, or the UCLA gravimeter record of the 1964 Alaskan earthquake (Benioff *et al.*, 1961; Alsop *et al.*, 1961; Ness *et al.*, 1961; Smith, 1961, 1972; Slichter, 1967; Geller and Stein, 1977; Stein and Geller, 1978a, b; Buland and Gilbert, 1978; Sailor and Dziewonski, 1978). However, these measurements are limited by the availability of only a single high-quality ultra-long period record for each event, and by the relatively high noise level of the instrument.

With the installation of the IDA network (Agnew *et al.*, 1976) of ultra-long period gravimeters, it is now possible to make attenuation measurements at many stations for a single earthquake. Since the signal-to-noise ratio of the IDA system is superior to older instruments, it is now possible to study modes with periods longer than 300 sec from records of earthquakes like the 1977 Indonesian earthquake with seismic moments on the order of 10 per cent of the great Alaskan or Chilean earthquakes.

In this paper, we use IDA records of the 1977 Indonesian earthquake to measure the attenuation of fundamental spheroidal modes from $_0S_6$ (962 sec) to $_0S_{28}$ (275 sec). We do not discuss the longest period spheroidal modes, $_0S_2$ through $_0S_5$, which

are split by the Earth's rotation and ellipticity. In order to measure the attenuation of these split modes, it is necessary to include the effects of the source mechanism, location and depth, and the receiver location (Stein and Geller, 1977, 1978a, b). These IDA records have been used to measure the attenuation of ${}_0S_0$ and ${}_1S_0$ by Buland *et al.* (1979).

The August 19, 1977 (M_S $7\frac{3}{4}$) earthquake occurred near Sumbawa, Indonesia. We used records of this event from seven IDA stations: Nana, Peru (NNA); Halifax, Nova Scotia (HAL); College, Alaska (CMO); Sutherland, South Africa (SUR); Raratonga, Cook Islands (RAR); Brasília, Brazil (BDF), and Garm, USSR (GAR). The relative geographical positions of the source and receivers are shown in Figure 1. The raw data are from the "mode" channel of the IDA instrument. Data on this channel are filtered to reduce the amplitudes of signals with a period of greater than 1 hr before digitization. Even after filtering, the amplitude of the solid Earth tide is still quite large. We have removed the tide by twice subtracting a $1\frac{1}{2}$-hr running

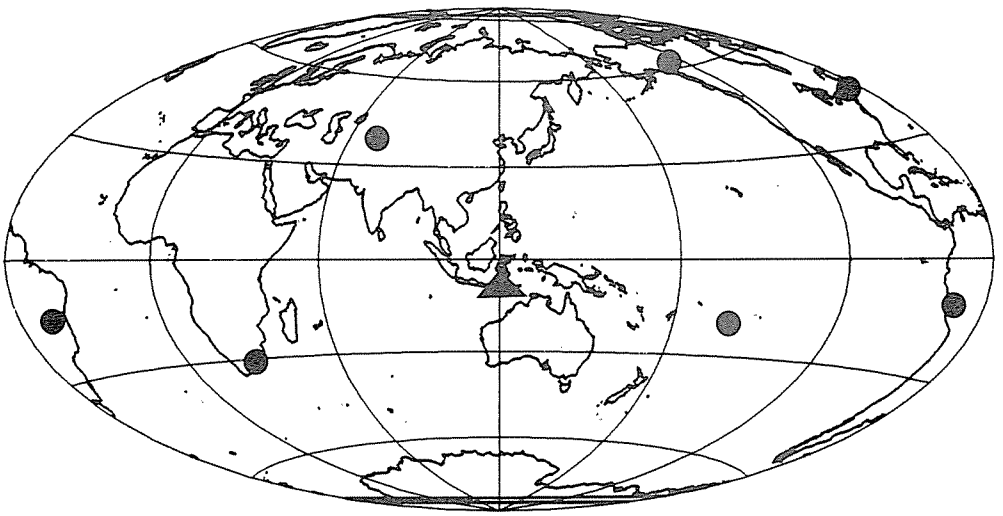

FIG. 1. Map showing the 1977 Indonesian earthquake (triangle) and IDA stations we used (circles).

average from the data. Prior to this, we deleted the earliest parts of each record, which were all saturated by large amplitude high-frequency surface waves. This procedure also eliminates possible aliasing, because the data are sampled at 20-sec intervals and the mode channel filter still has non-negligible gain at frequencies higher than the Nyquist (0.025 Hz).

The starting time varies from record to record, and all but SUR and GAR extend to 140 hr after the earthquake. At some stations two successive casettes were chained together to obtain a long enough record. The gap (about 20 min) between casettes was filled with zeroes. The data at GAR beyond about 60 hr are unusable because of noise resulting from the flooding of a nearby river (R. Buland, personal communication, 1978). The Sutherland record is shorter than any of the others but GAR because the mass was physically rezeroed at the beginning and end of the record. The portions of the record we used in our study, after detiding, are shown in Figure 2. Several aftershocks and local earthquakes are clearly visible on the records

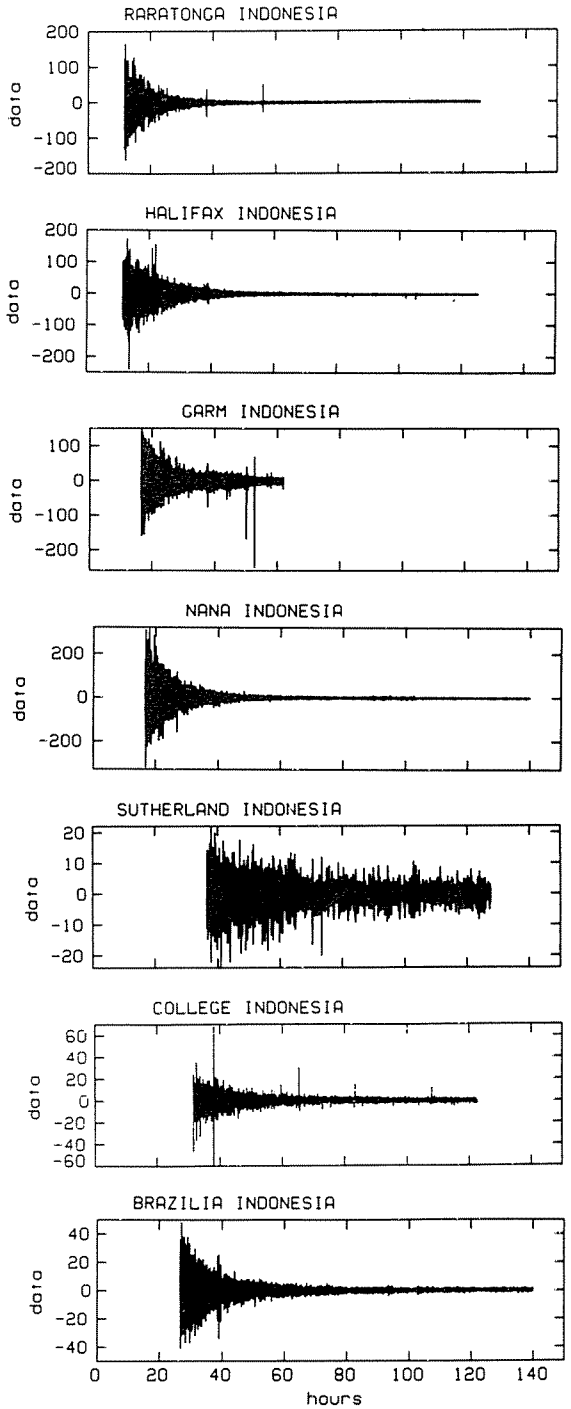

FIG. 2. IDA records of the Indonesian earthquake after removal of the earth tide and of clipped portions of the data. Amplitudes are in digital units.

in Figure 2. We decided not to remove these signals, after some experiments which showed that no improvement resulted.

Spectra for all seven records are shown in Figure 3. They were obtained by decimating (and smoothing) the time series in Figure 2 to no more than 7,192 points, tapering 10 per cent at either end with a cosine window, and then padding with enough zeroes to get 8,192 points. The fundamental spheroidal modes have excellent signal-to-noise ratios. Splitting can be seen for ${}_0S_2$ to ${}_0S_5$ and many overtones are clearly visible. The radial modes ${}_0S_0$ and ${}_1S_0$ are also visible. The unsplit spheroidal modes ${}_0S_6$ to ${}_0S_{28}$, which we studied, have good signal-to-noise on most records. Some modes (e.g., ${}_0S_{27}$ at CMO) are not well recorded at a given station, and were excluded from our analysis.

Time Domain Attenuation Measurements

The major advantages of time-domain measurement are in its ability to minimize the effects of various types of noise. By studying the decay of the amplitude of a mode as a function of time, it is possible to directly determine the quality of the observation, in ways not possible in the frequency domain. A damped harmonic oscillator, recorded with no noise, will show a standard resonance peak in the frequency domain or exponentially decaying amplitude in the time domain; its attenuation can be measured in either domain with equal facility. However, as noise is introduced, it is almost impossible to determine the amount of noise contamination in the frequency domain. On the other hand, the extent to which the signal in the time domain differs from a pure decaying exponential provides a straightforward way to determine the quality of an observation. A noise burst, resulting from an aftershock or some other source of contamination, will be easily detectable from the scalloping of the exponential decay; such biased observations can therefore be rejected. (Computing the power in successive windows, a seemingly equivalent method, is actually much less effective in detecting such effects.) Another advantage of time-domain measurements is that they allow immediate identification of the ambient noise level, and signals at or below this level can be disregarded. The details of our procedure are discussed below.

Starting with the Fourier transform of a tapered time series, we then narrow-band filter the transform to isolate a particular mode, using a zero-phase filter with unit gain in the passband and 5 per cent cosine tapering at either end of the window. (Other narrow-band filter windows appear to yield roughly similar results.) The narrow-band filtered transform is then inverse transformed to obtain the time series for the mode, and its Hilbert transform. We then plot the logarithm of the analytic signal, which represents the decay of the envelope of the mode as a function of time. Q^{-1} is then determined from the slope of straight lines fit to the envelope using least squares.

It is far preferable to state the attenuation measurement in terms of Q^{-1} rather than in terms of Q. Q^{-1} is the quantity actually measured from the slope of the line and the most natural quantity to use in inverting for attenuation as a function of depth. Finally, because attenuation is always quite low, any discussion posed in terms of Q, rather than Q^{-1}, tends to exaggerate small differences. (The difference between $Q = 100$ and $Q = 1{,}000$ is $\Delta(Q^{-1}) = 0.009$, while the difference between $Q = 1{,}000$ and $Q = 10{,}000$ is only $\Delta(Q^{-1}) = 0.0009$. Although the latter difference is actually ten times smaller, this tends to be overlooked in practice.)

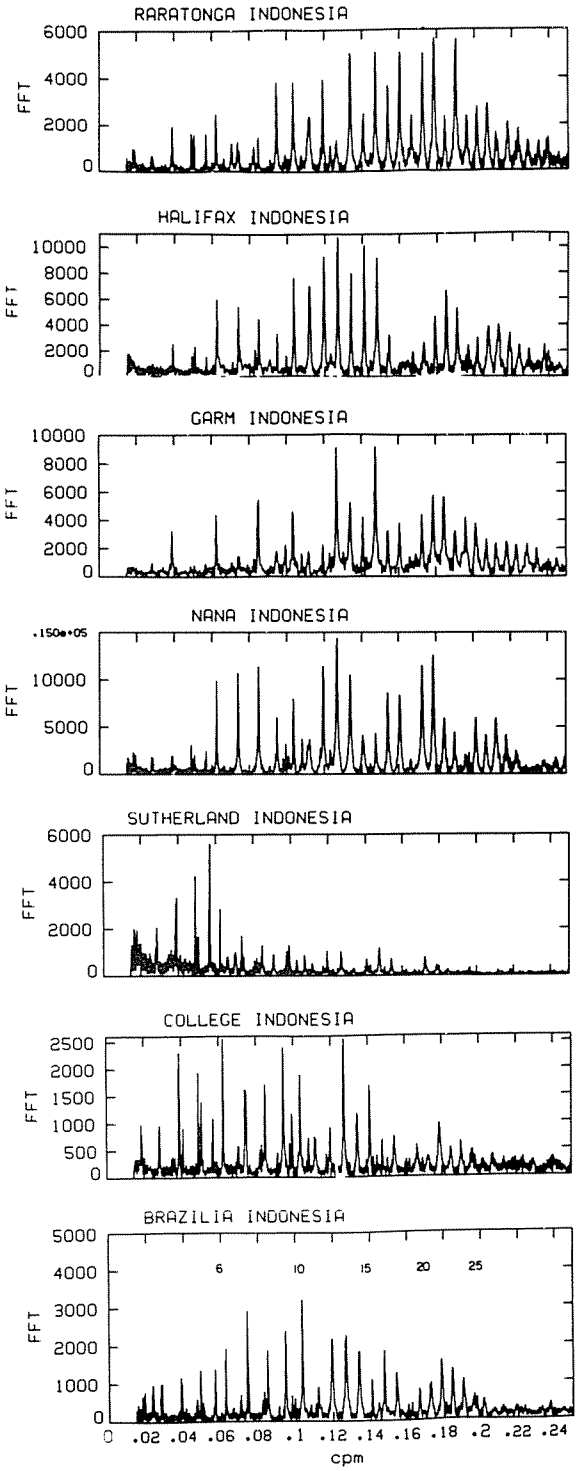

FIG. 3. Spectra of the IDA records of the Indonesian earthquake which we used for our Q^{-1} study. The angular orders of the fundamental spheroidal modes are shown at the top of the Brasília record.

Test Cases

Our time-domain measurement procedure was tested on synthetic-mode data, both to test the programs used for the analysis and to study the effects of noise. A synthetic time series was constructed consisting of the sum of two modes with different frequencies and Q^{-1} (Figure 4). The synthetic starts 10 hr after the origin time and extends for 90 hr. The two modes have periods of 600 and 450 sec, and Q's of 500 and 250, respectively.

The synthetics were processed in the same way as the data. First, we removed the "tide" by twice subtracting the running average (which essentially has no effect for the synthetic), then tapered and Fourier transformed to obtain the spectrum. Each of the two modes was then narrow-band filtered to produce the two decaying envelopes shown on the *right* side of Figure 4. The format of these two envelope

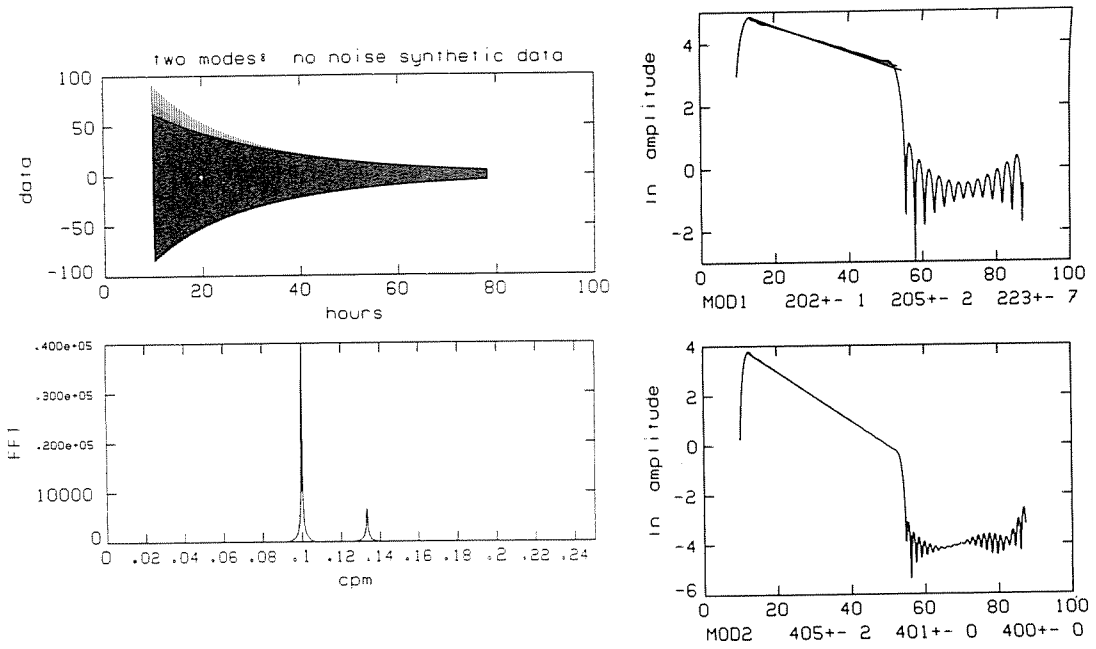

FIG. 4. Test of the time domain Q^{-1} measurements for synthetic without noise. Details of the Q^{-1} plots (*right*) are given in the caption for Figure 6.

plots is identical to those used later for the actual data. The x-axis is time, in hours; the y-axis is the (natural) logarithm of the amplitude, in digital units.

Q^{-1} is measured by fitting straight lines to segments of the data ranging from the time of the peak amplitude until the time that the signal decays to e^{-1}, e^{-2}, and e^{-3} of the peak, respectively. Q^{-1} is then given by

$$Q^{-1} = -\bar{m}T/\pi$$

where T is the period of the mode and $\bar{m}$ is the slope of the line. Thus there are three Q^{-1} estimates for each mode, corresponding to the three least-squares lines shown. The numbers below the x-axis from left to right are actually $Q^{-1} \times 10^5$, for each of the three lines. In this case there was no noise and the exact answers, as obtained, are 200 and 400, respectively The standard deviations shown for each Q^{-1}

value are obtained from the standard least-squares formula, using twice the number of frequency points in the passband as the number of degrees of freedom. Such least-squares standard deviations tend to significantly underestimate the uncertainty of the results. As discussed below, the differences between Q^{-1} measurements at different receivers is a better measure of the error.

We also tested our method by adding noise to the synthetic data (Figure 5). At each time point noise uniformly distributed between ±15 digital units was added. The filtered time series are somewhat degraded, but the time-domain attenuation measurements are still successful.

Results

Our method was applied to the seven IDA records shown in Figure 2. Amplitude decay plots were prepared for the 23 modes from ${}_0S_6$ to ${}_0S_{28}$. The filter passbands for

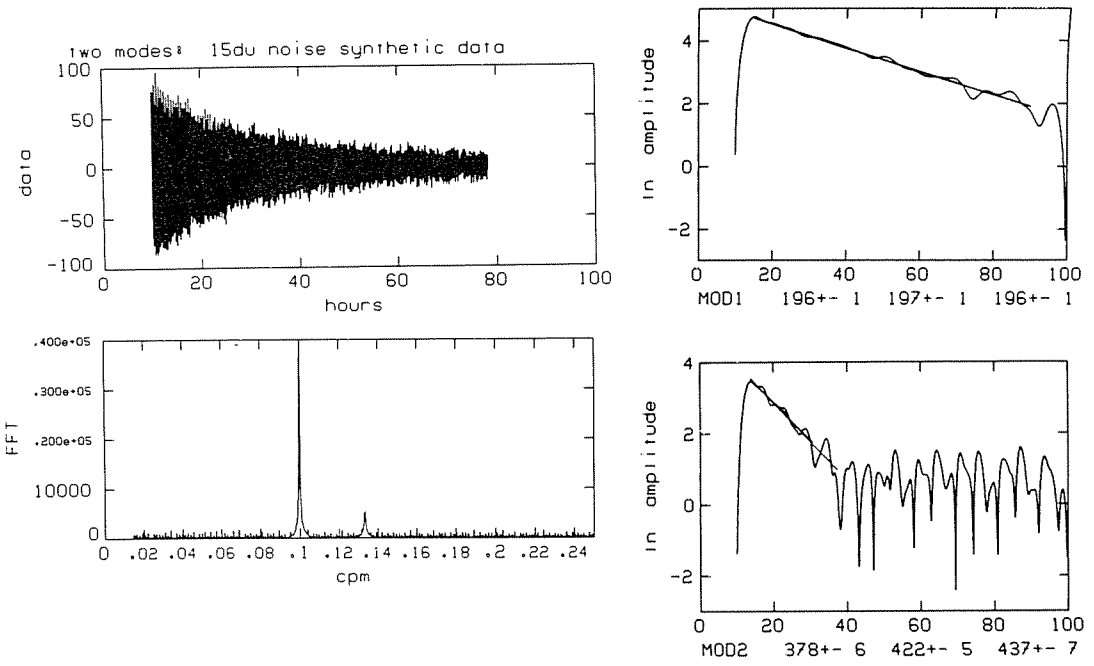

FIG. 5. Same as Figure 4, for a synthetic with random white noise.

each mode are given in Table 1. Plots of the envelope were made for each mode at each station, but only those records in which the amplitude decayed smoothly as a function of time were used. These Q^{-1} measurements are shown in Figures 6 through 14. In occasional cases, the e^{-1} straight line was obviously biased by a local amplitude minimum which did not affect the e^{-2} or e^{-3} lines. In such cases, only the Q^{-1} values corresponding to the last two measurements are shown. Different numbers of stations had sufficiently high-data quality for each mode. In one case, ${}_0S_{11}$, none of the data were acceptable. Because the amplitude scale is logarithmic, the noise at the end of some records is of negligible amplitude. Some of the very low-amplitude noise is the result of the zero fill at the end of the records. In general, the data are extremely good, and the values of Q^{-1} for each record (shown $\times 10^5$) are very well constrained.

By deleting data where the amplitude decay is not smooth, we reject several sources of error. One such case is when an overtone, within the frequency window of the mode, is well excited. The noisy amplitude decay correlates with a strong overtone peak in the amplitude spectrum. For example, ${}_0S_7$ (811 sec) is seriously contaminated by ${}_2S_3$ (804 sec) at GAR, RAR, SUR, and CMO (Figure 15).

Our difficulties with ${}_0S_{11}$, where no usable records were obtained, may be due to coupling between ${}_0S_{11}$ and ${}_0T_{12}$ (Luh, 1974; Chao and Gilbert, 1979).

We have neglected the effect of splitting due to lateral heterogeneity, where the individual singlets are not observable as separate peaks because of attenuation and record length (Dahlen 1976, 1979). This effect may cause differences in eigenfrequency (Jordan, 1978) and attenuation (Buland, in preparation) at different stations.

The error estimate from the least-squares fit indicates the precision of the attenuation measurement at each station. The differences between stations then

TABLE 1

FILTER PASSBANDS

Mode	Period Range (sec)
0S6	983.00–937.00
0S7	840.00–780.00
0S8	721.00–693.00
0S9	643.00–619.00
0S10	593.00–566.00
0S11	541.00–530.00
0S12	509.00–491.00
0S13	492.00–464.00
0S14	455.00–441.00
0S15	428.00–422.00
0S16	410.00–402.00
0S17	393.00–384.00
0S18	375.00–370.40
0S19	365.80–355.00
0S20	353.00–342.40
0S21	340.20–331.10
0S22	329.70–321.20
0S23	319.10–311.20
0S24	308.00–304.20
0S25	302.50–295.20
0S26	293.60–285.70
0S27	285.70–281.90
0S28	276.80–274.20

indicate the uncertainty of the average global measurement of attenuation. A significant fraction of this uncertainty may be due to lateral heterogeneity because the differences between stations are much greater than the uncertainty of most individual single station measurements. With additional data from other earthquakes, it may be possible to resolve true lateral heterogeneity in attenuation.

Lateral heterogeneity affects the Q^{-1} of individual singlets in a complicated way which depends on the eigenfunctions of each singlet. Present methods for calculating the modes of a laterally heterogeneous earth model, primarily relying on first-order perturbation theory, do not calculate the eigenfunctions with the necessary accuracy to make studies of the lateral heterogeneity of Q^{-1}. By analogy to a one-dimensional laterally heterogenous body (Geller and Stein, 1978), it is probably necessary to use variational methods to obtain the necessary accuracy.

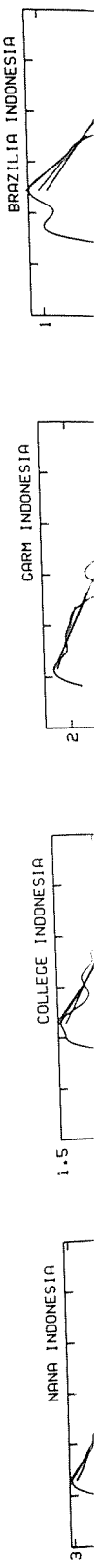

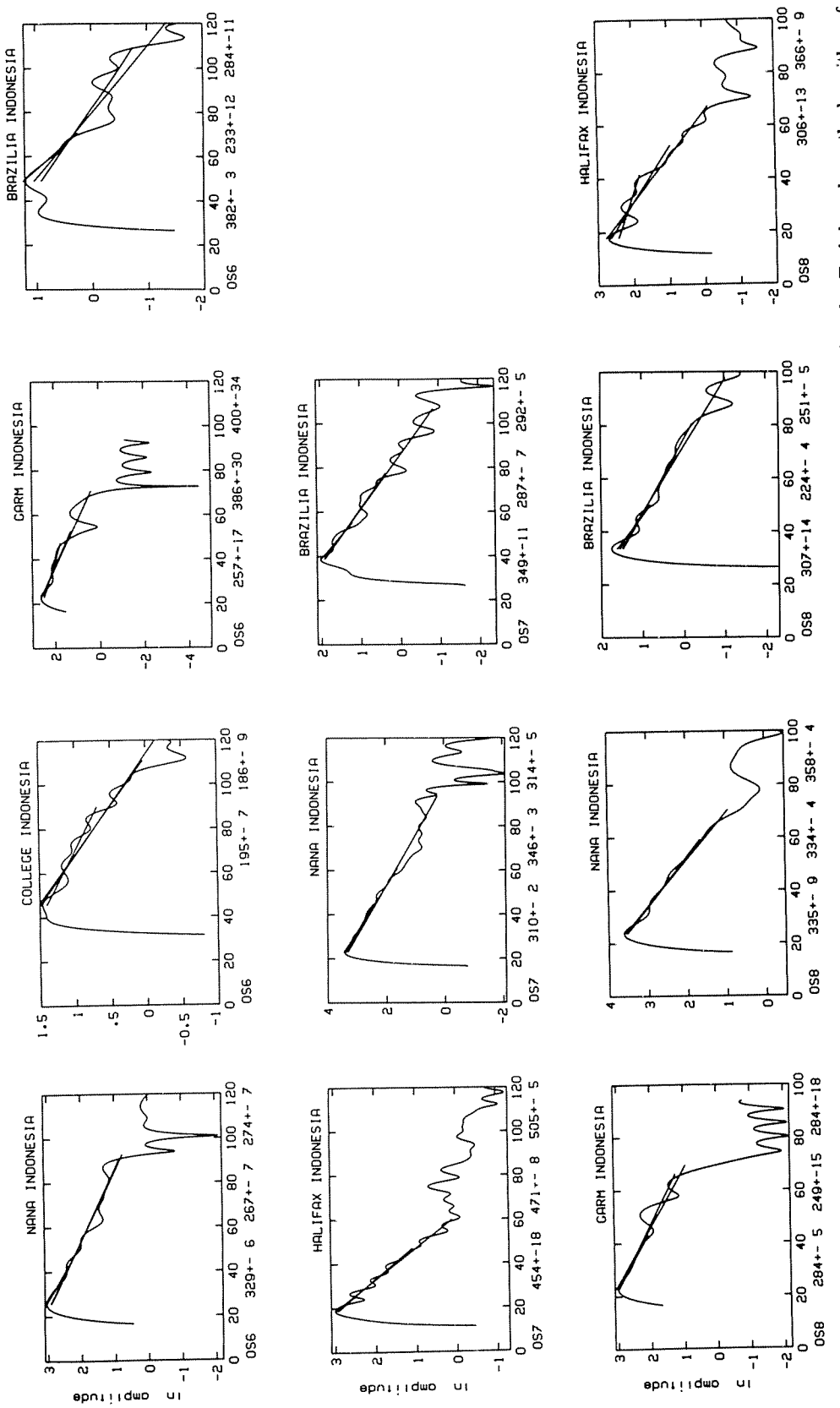

FIG. 6. Fundamental spheroidal mode Q^{-1} measurements for ${}_0S_6$, ${}_0S_7$, and ${}_0S_8$ from the IDA records of the Indonesian earthquake. Each box shows the logarithm of (unsmoothed) envelope for a particular mode (vertical scale) observed at a particular receiver, decaying as a function of time (in hours after the origin time). The three numbers on the same line as the mode identification show $Q^{-1} \times 10^5$ from the e^{-1}, e^{-2}, and e^{-3} least-squares lines. Error bounds are nominal, from the least-squares formula. Occasionally (e.g., ${}_0S_6$ at College) the e^{-1} value is unreliable and not shown.

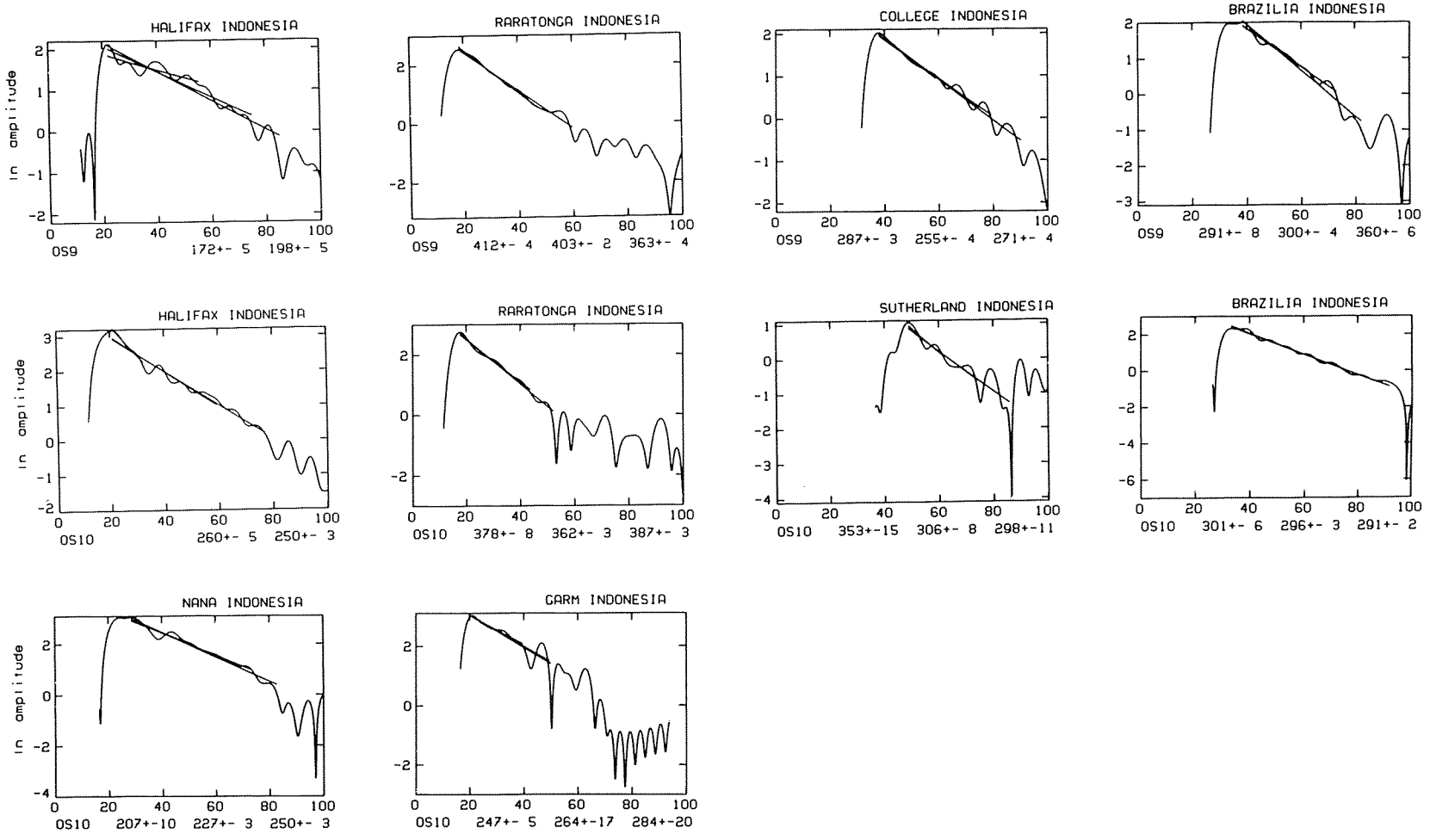

FIG. 7. Same as Figure 6 for ${}_0S_9$ and ${}_0S_{10}$.

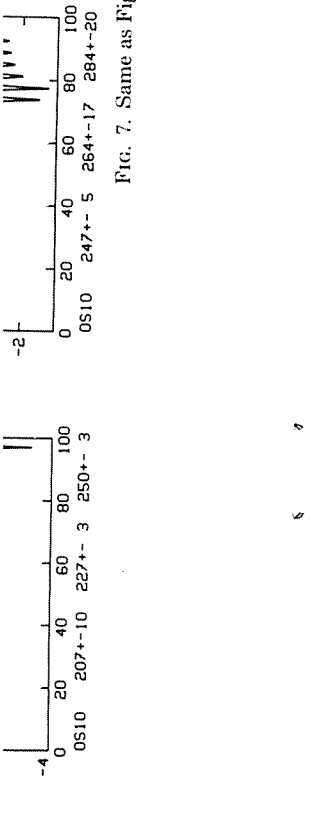

FIG. 7. Same as Figure 6 for ${}_0S_9$ and ${}_0S_{10}$.

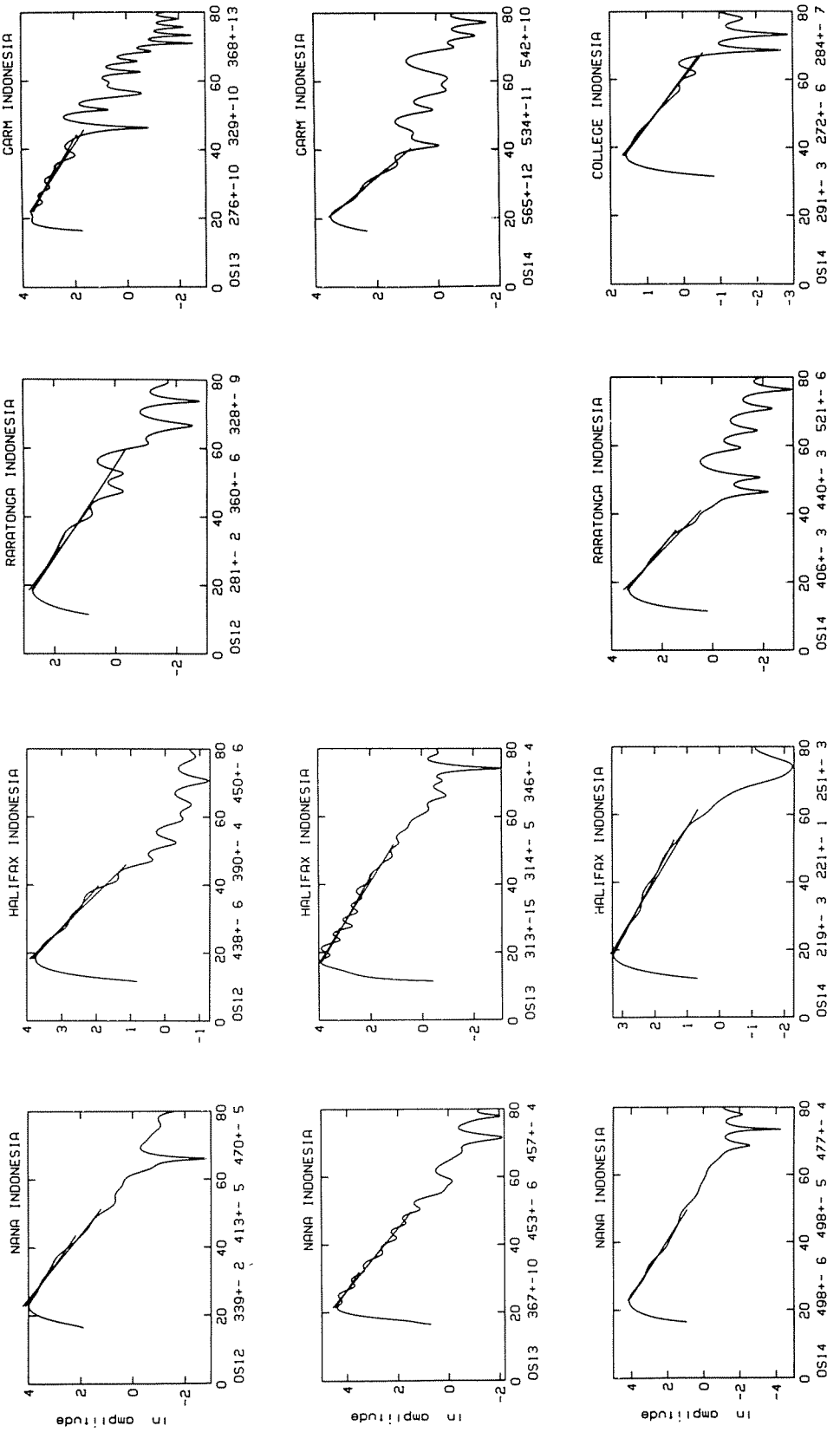

FIG. 8. Same as Figure 6 for ${}_0S_{12}$, ${}_0S_{13}$, and ${}_0S_{14}$.

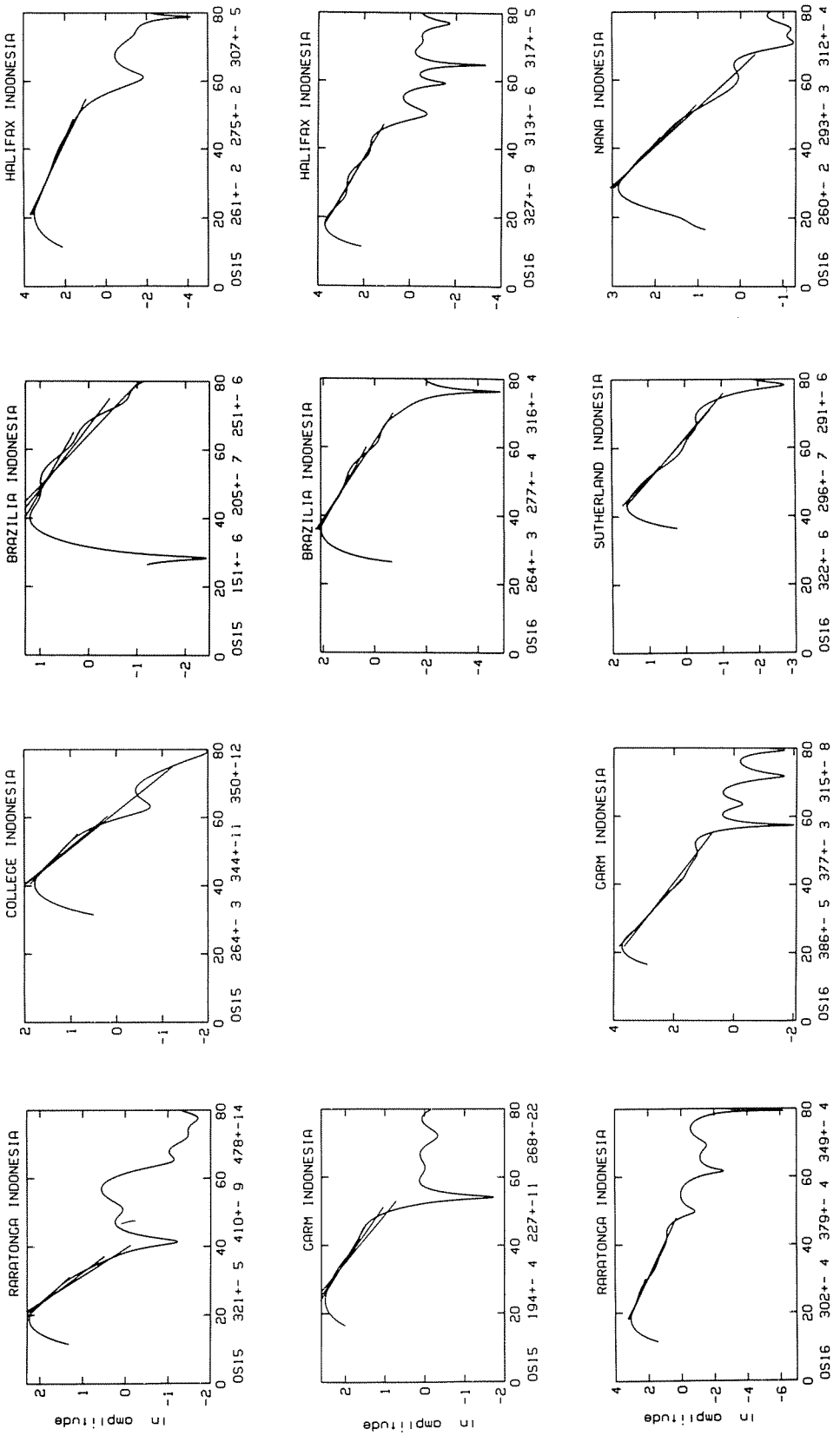

FIG. 9. Same as Figure 6 for ${}_0S_{15}$ and ${}_0S_{16}$.

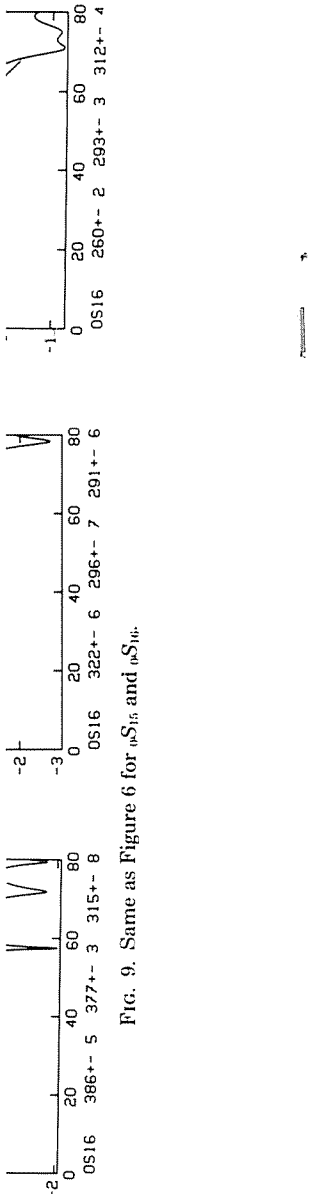

FIG. 9. Same as Figure 6 for ${}_{\mu}S_{15}$ and ${}_{\mu}S_{16}$.

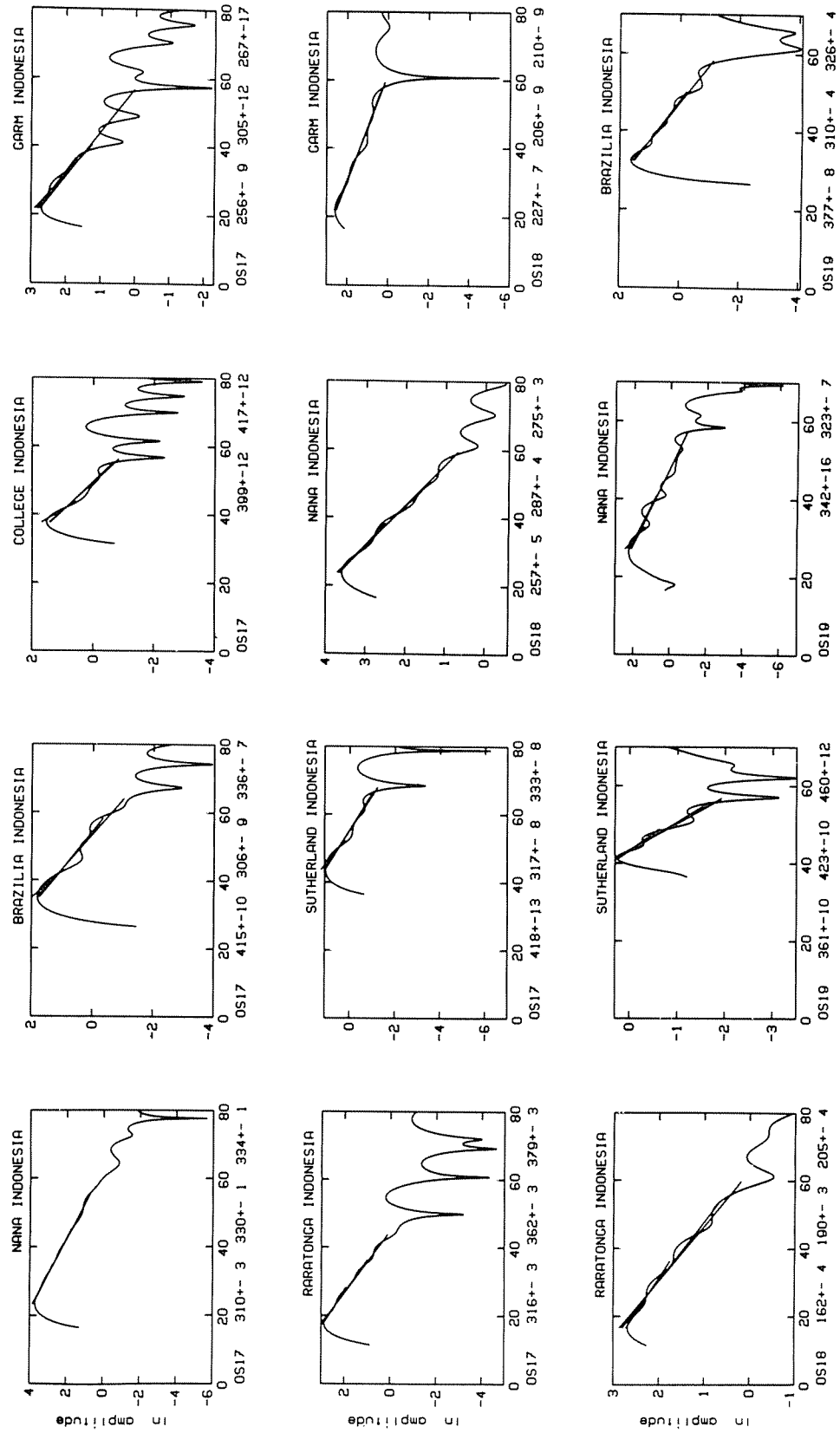

FIG. 10. Same as Figure 6 for ${}_{\mu}S_{17}$, ${}_{\mu}S_{18}$, and ${}_{\mu}S_{19}$.

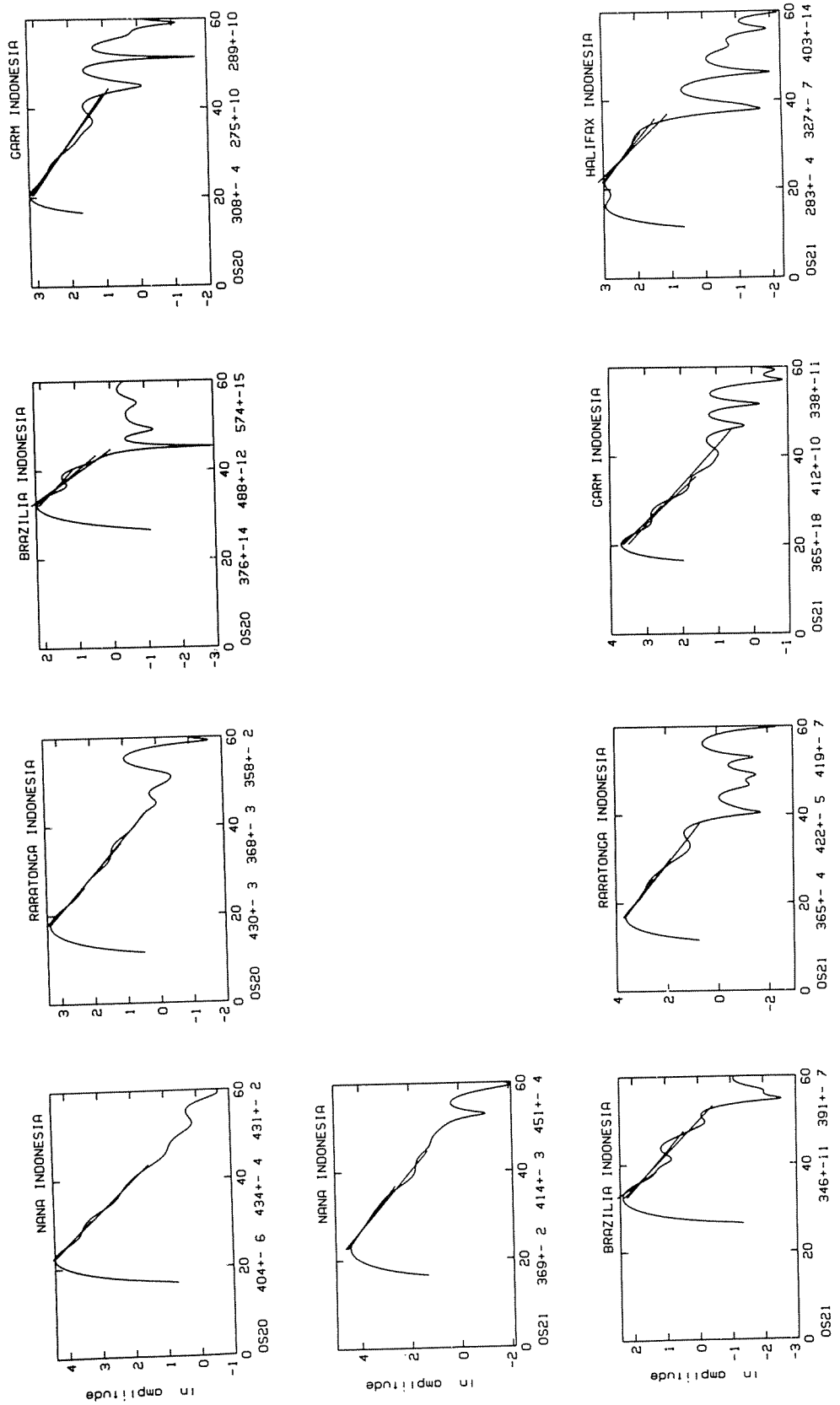

FIG. 11. Same as Figure 6 for ${}_0S_{20}$ and ${}_0S_{21}$.

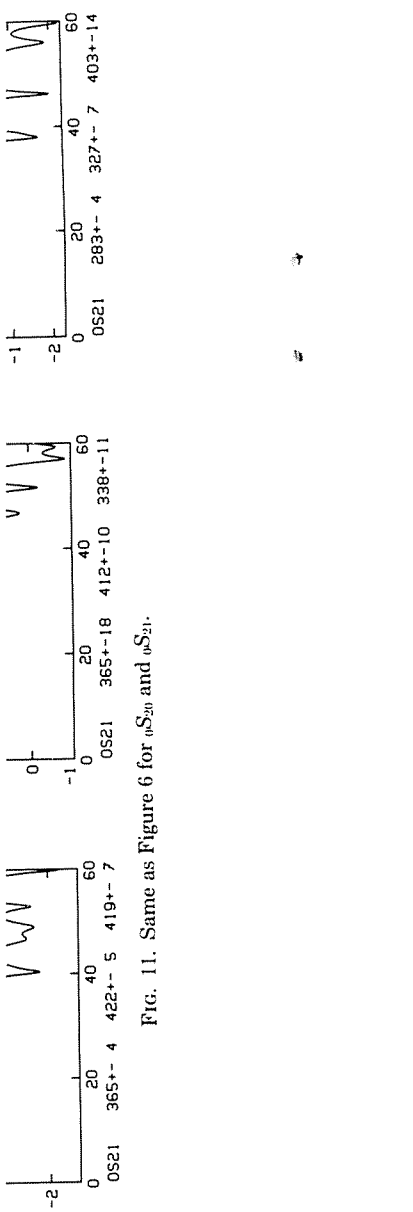

FIG. 11. Same as Figure 6 for ${}_{0}S_{20}$ and ${}_{0}S_{21}$.

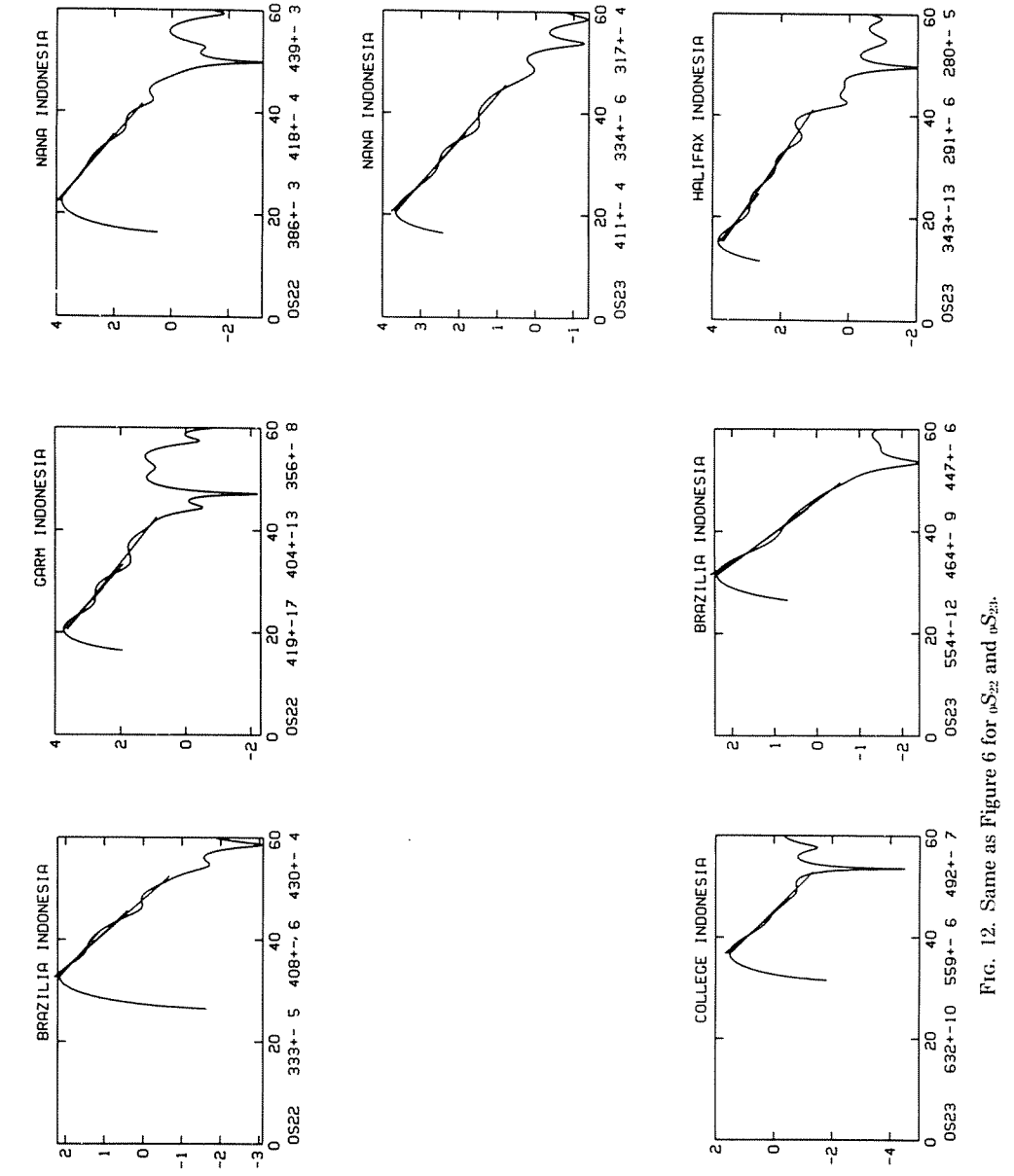

FIG. 12. Same as Figure 6 for ${}_{0}S_{22}$ and ${}_{0}S_{23}$.

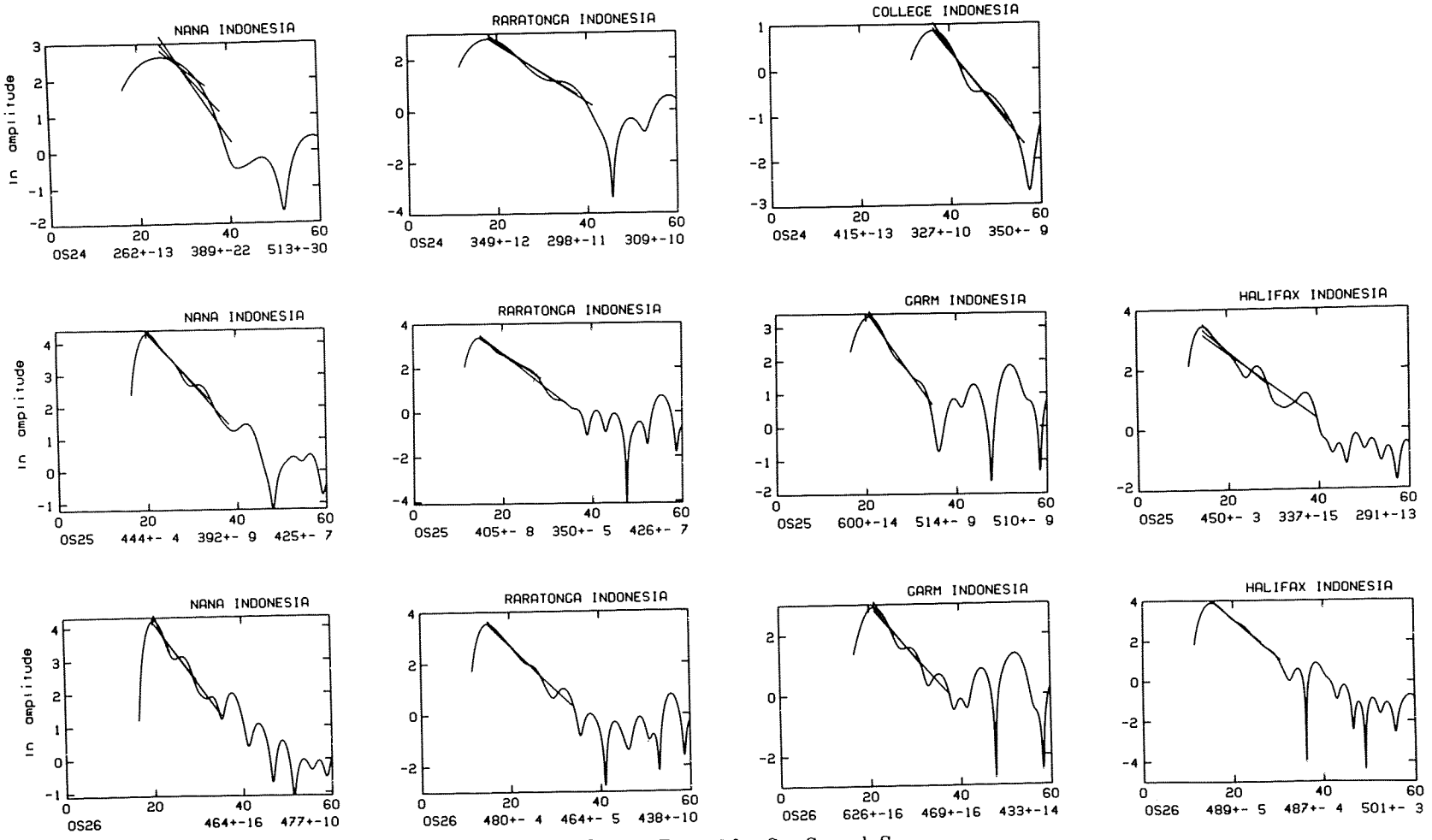

FIG. 13. Same as Figure 6 for ${}_0S_{24}$, ${}_0S_{25}$, and ${}_0S_{26}$.

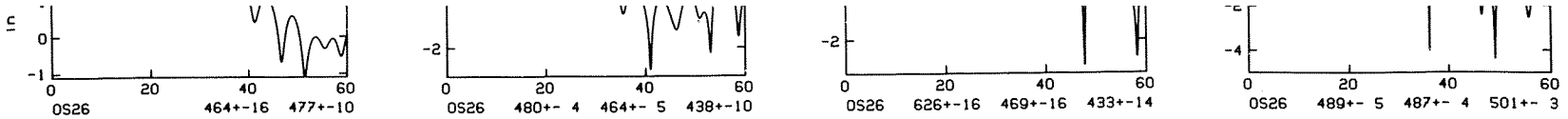

FIG. 13. Same as Figure 6 for ${}_0S_{24}$, ${}_0S_{25}$, and ${}_0S_{26}$.

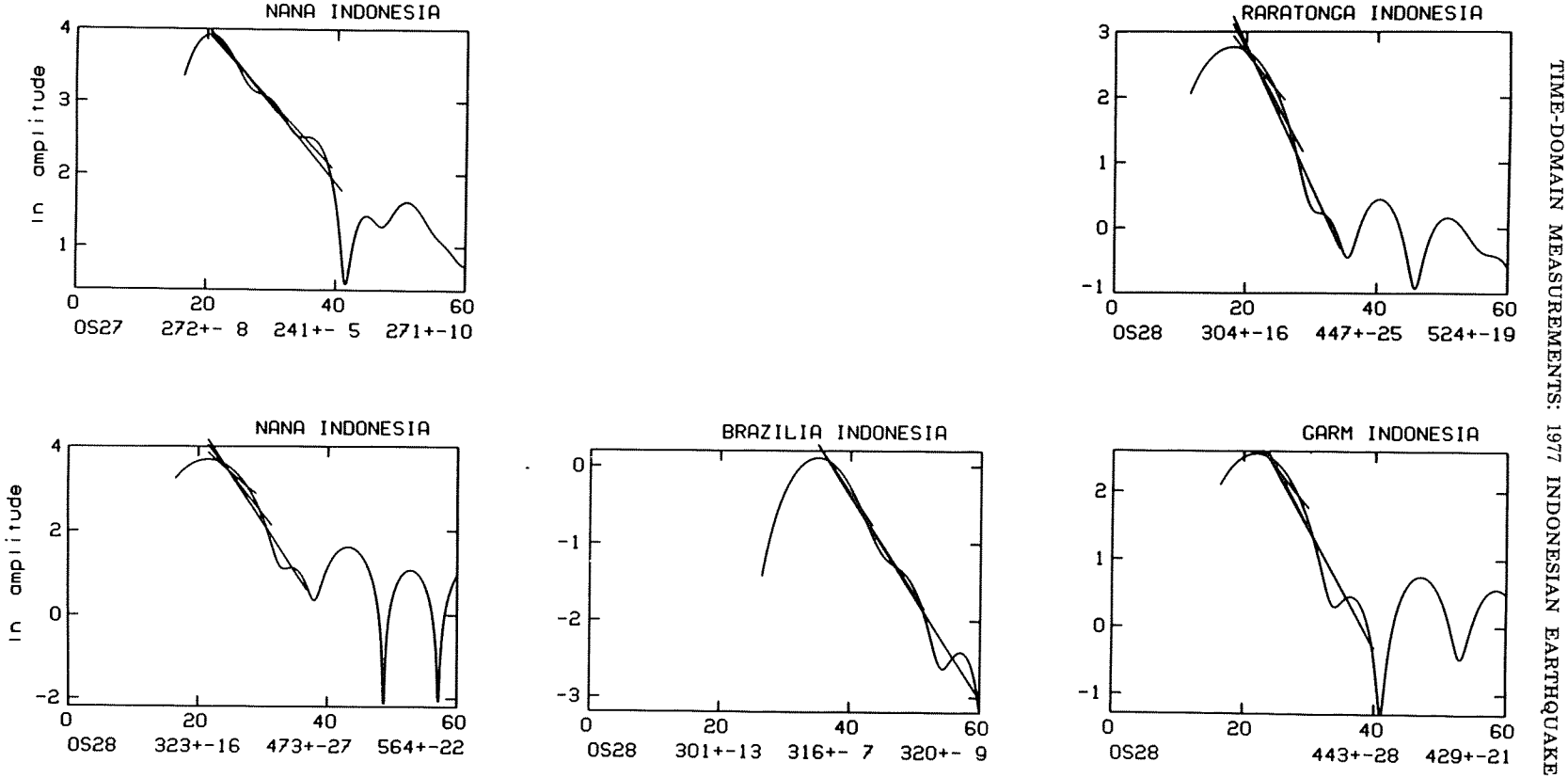

FIG. 14. Same as Figure 6 for ${}_0S_{27}$ and ${}_0S_{28}$.

Discussion

Table 2 lists the mean of the Q^{-1} values at each station and the mean of all the Q^{-1} measurements for each mode. The standard deviation shown for each global mean is obtained from the misfit of the individual single station measurements. Because different stations were available for different modes, there conceivably are some systematic biases. However, there are no differences between stations above the background scatter.

The Q^{-1} measurements at each station are plotted in Figure 16, and the mode means are plotted in Figure 17. Also shown in Figure 17 are the Q^{-1} data of Sailor

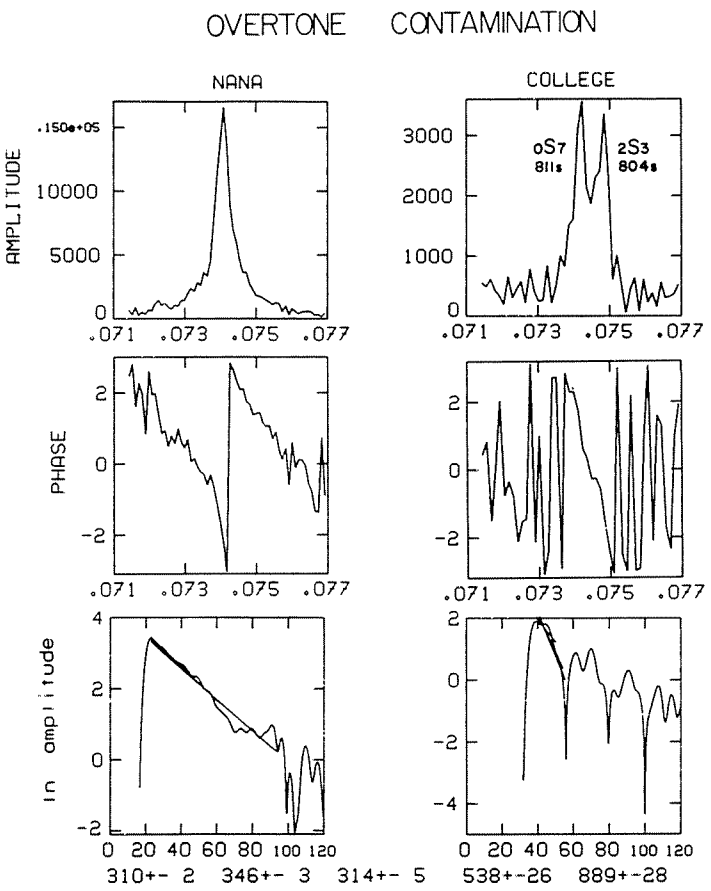

FIG. 15. Effect of overtone interference on ${}_0S_7$. At College, ${}_0S_7$ is contaminated by ${}_2S_3$, as shown by the phase and amplitude spectra, while at Nana, ${}_0S_7$ is not affected. The amplitude decay plot at College is unusable.

and Dziewonski (1978), both for gravimeter measurements and for stacked WWSSN seismograms, the value for ${}_0S_2$ of Buland and Gilbert (1978), and our previous (Stein and Geller, 1978b) measurements for split modes ${}_0S_2$ to ${}_0S_5$ for the Chilean and Alaskan earthquakes. Their gravimeter data are in accord with ours, while the stacked records give higher Q^{-1}. Sailor and Dziewonski noted that stacking could result in systematically high Q^{-1}, but at the time of their study no better dataset was available. They also pointed out the difficulty of estimating the uncertainty in the measurements, given a single value.

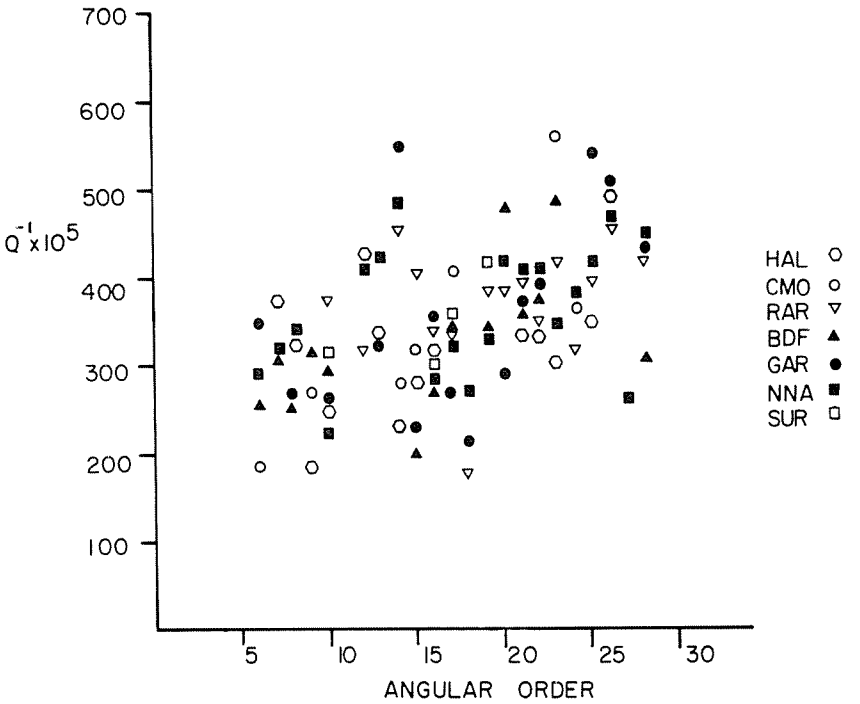

FIG. 16. Q^{-1} measurements from Table 1.

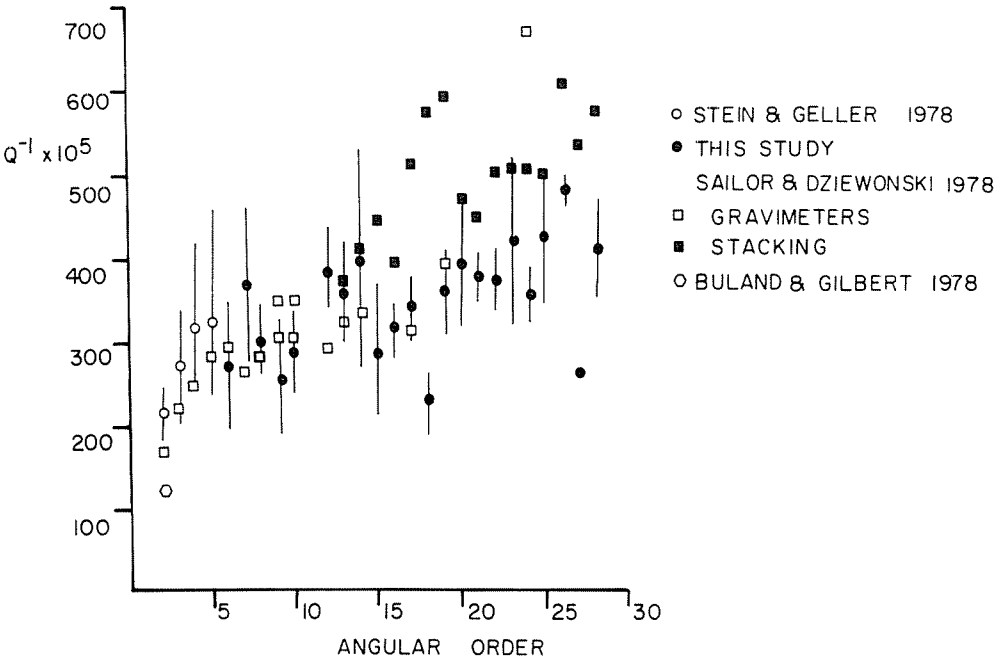

FIG. 17. Fundamental spheroidal mode Q^{-1} data from Stein and Geller (1978b), open circles; this study, closed circles; the error bars refer to our results. Note that there is very good agreement with Sailor and Dziewonski's (1978) single-station gravimeter Q^{-1} results, but that their stacking results from WWSSN data show systematically higher Q^{-1}.

Our dataset consists of Q^{-1} measurements from ${}_0S_6$ to ${}_0S_{28}$ for seven IDA records of the 1977 Indonesian earthquake. We could measure Q^{-1} for 21 of these modes for at least three stations. Within the present error bars for Q^{-1} data, the agreement between our results, Sailor and Dziewonski's (1978), and Bolt and Hansen's (1979) results is very good. Our measurements have greatly increased the number of reliable Q^{-1} data in the band from about 900 to 300 sec. We discuss the implications for gross Earth Q^{-1} structure elsewhere (Mills *et al.*, 1979).

TABLE 2

ATTENUATION (100,000/Q)

	Garm	Nana	College	Brasília	Halifax	Sutherland	Raratonga	Average
${}_0S_6$	348	290	190	258	—	—	—	272 ± 66
${}_0S_7$	—	323	—	309	477	—	—	370 ± 93
${}_0S_8$	272	342	—	261	336	—	—	303 ± 42
${}_0S_9$	—	—	271	317	185	—	—	258 ± 67
${}_0S_{10}$	265	228	—	296	255	319	376	290 ± 53
${}_0S_{11}$	—	—	—	—	—	—	—	—
${}_0S_{12}$	—	407	—	—	426	—	323	385 ± 55
${}_0S_{13}$	324	426	—	—	324	—	—	358 ± 59
${}_0S_{14}$	547	491	282	—	230	—	456	401 ± 138
${}_0S_{15}$	230	—	319	202	281	—	403	287 ± 59
${}_0S_{16}$	359	288	—	286	319	303	343	316 ± 30
${}_0S_{17}$	276	325	408	352	—	356	352	345 ± 43
${}_0S_{18}$	214	273	—	—	—	—	186	224 ± 44
${}_0S_{19}$	—	332	—	338	—	415	—	362 ± 46
${}_0S_{20}$	291	423	—	479	—	—	385	395 ± 79
${}_0S_{21}$	372	411	—	368	338	—	402	378 ± 29
${}_0S_{22}$	393	414	—	390	336	—	351	377 ± 32
${}_0S_{23}$	—	354	561	488	305	—	419	425 ± 102
${}_0S_{24}$	—	388	364	—	—	—	319	357 ± 35
${}_0S_{25}$	541	420	—	—	359	—	394	429 ± 79
${}_0S_{26}$	509	470	—	—	492	—	461	483 ± 22
${}_0S_{27}$	—	261	—	—	—	—	—	261 —
${}_0S_{28}$	436	453		312	—	—	425	407 ± 64

ACKNOWLEDGMENTS

We thank Ray Buland and Freeman Gilbert for providing us with the IDA data and information about the records. We also thank Joe Mills, Howard Patton, and Richard Sailor for useful discussions, and Einar Kjartansson for help in reading the IDA tapes. We have benefited from a careful review by Ray Buland. This work was supported by NSF Grant EAR 78-03653.

REFERENCES

Agnew, D., J. Berger, R. Buland, W. Farrell, and F. Gilbert (1976). International deployment of accelerometers: a network for very long period seismology, *EOS Trans. Am. Geophys. Union* **57,** 180–188.

Alsop, L. E., G. Sutton, and M. Ewing (1961). Free oscillations of the earth observed on strain and pendulum seismographs, *J. Geophys. Res.* **66,** 621–629.

Benioff, H., F. Press, and S. Smith (1961). Excitation of the free oscillations of the earth, *J. Geophys. Res.* **66,** 605–619.

Bolt, B. A. and R. A. Hansen (1979). Variations between Q values estimated from damped terrestial eigenvibrations, in *Proc. Conf. Seismic Wave Attenuation*, Standford Univ. 11–12.

Buland, R. and F. Gilbert (1978). Improved resolution of complex eigenfrequencies in analytically continued spectra, *Geophys. J.* **52,** 457–470.

Buland, R., J. Berger, and F. Gilbert (1979). Observations of attenuation and splitting from the IDA network, *Nature* **277,** 358–362.

Chao, B. and F. Gilbert (1979). Multimode estimation of complex eigenfrequencies (abstract), *EOS Trans. Am. Geophys. Union* **60,** 324.

Dahlen, F. A. (1976). Models of the lateral heterogeneity of the Earth consistent with eigenfrequency splitting data, *Geophys. J.* **44,** 77–106.

Dahlen, F. A. (1979). The spectra of unresolved split normal mode multiplets, *Geophys. J.* **58,** 1–33.

Geller, R. J. and S. Stein (1977). Split free oscillation amplitudes for the 1960 Chilean and 1964 Alaskan earthquakes, *Bull. Seism. Soc. Am.* **67,** 651–660.

Geller, R. J. and S. Stein (1978). Normal modes of a laterally heterogeneous body: A one-dimensional example, *Bull. Seism. Soc. Am.* **68,** 103–116.

Jordan, T. H. (1978). A procedure for estimating lateral variations from low-frequency eigenspectra data, *Geophys. J.* **52,** 441–456.

Kanamori, H. (1970). Velocity and Q of mantle waves, *Phys. Earth Planet. Interiors* **2,** 259–275.

Luh, P. C. (1974). Normal modes of a rotating self-gravitating inhomogenous Earth, *Geophys. J.* **38,** 187–224.

Mills, J. M. (1978). Great-circle Rayleigh wave attenuation and group velocity, part IV: Regionalization and pure-path models for shear velocity and attenuation, *Phys. Earth Planet. Interiors* **17,** 323–352.

Mills, J. M. and A. L. Hales (1977). Great-circle Rayleigh wave group velocities and attenuation coefficients, Part I: Observations for periods between 150 and 600 seconds for seven great circle paths, *Phys. Earth Planet. Interiors* **14,** 109–119.

Mills, J. M. and A. L. Hales (1978a). Great circle Rayleigh wave group velocities and attenuation coefficients, Part II: Observations between 50 and 200 seconds and global averages for periods of 50 to 600 seconds, *Phys. Earth Planet. Interiors* **17,** 209–231.

Mills, J. M. and A. L. Hales (1978b). Great-circle Rayleigh wave group velocities and attenuation coefficients, Part III: Inversion of global average group velocities and attenuation coefficients, *Phys. Earth Planet. Interiors* **17,** 307–322.

Mills, J. M., S. Stein, and R. J. Geller (1979). Attenuation measurements from free oscillations and surface waves and their implications, in *Proc. Conf. Seismic Wave Attenuation*, Stanford Univ. 4–5.

Mitchell, B. J., L. W. B. Leite, Y. K. Yu, and R. B. Herrmann (1976). Attenuation of Love and Rayleigh waves across the Pacific at periods between 15 and 110 seconds, *Bull. Seism. Soc. Am.* **66,** 1189–1202.

Nakanishi, I. (1978). Regional differences in the phase velocity and the quality factor Q of mantle Rayleigh waves, *Science* **200,** 1379–1381.

Ness, N., J. Harrison, and L. Slichter (1961). Observations of the free oscillations of the earth, *J. Geophys. Res.* **66,** 621–629.

Sailor, R. V. and A. M. Dziewonski (1978). Measurements and interpretation of normal mode attenuation, *Geophys. J.* **53,** 559–582.

Slichter, L. B. (1967). Spherical oscillations of the earth, *Geophys. J.* **14,** 171–177.

Smith, S. W. (1961). An investigation of the earth's free oscillations, *Ph.D. Thesis*, California Institute of Technology, Pasadena.

Smith, S. W. (1972). The anelasticity of the mantle, *Tectonophysics* **13,** 601–622.

Stein, S. and R. J. Geller (1977). Amplitudes of the split normal modes of a rotating, elliptical earth excited by a double couple, *J. Phys. Earth* **25,** 117–142.

Stein, S. and R. J. Geller (1978a). Time domain observation and synthesis of split-spheroidal and torsional free oscillations of the 1960 Chilean earthquake: preliminary results, *Bull. Seism. Soc. Am.* **68,** 325–332.

Stein, S. and R. J. Geller (1978b). Attenuation measurements of split normal modes for the 1960 Chilean and 1964 Alaskan earthquakes, *Bull. Seism. Soc. Am.* **68,** 1595–1011.

Tsai, Y. B. and K. Aki (1969). Simultaneous determination of the seismic moment and attenuation of seismic surface waves, *Bull. Seism. Soc. Am.* **54,** 275–287.

Department of Geophysics
Stanford University
Stanford, California 94305

Manuscript received May 8, 1979